Comparison of Geostrophically-Derived and ADCP Current Velocity in the Upper 600 Meters of the Equatorial Pacific

Kayla Robertson

University of Washington, Seattle

School of Oceanography

krob711@uw.edu

Abstract

Geostrophic balance, a fundamental concept describing the equilibrium between Coriolis forces and pressure gradients, influences current patterns in the ocean. However, at the equator, the absence of Coriolis forces impacts current predictions using standard equations. Measurements were taken on research cruise TN427 on the R/V Thomas G. Thompson, from 28 December 2023 to 11 January 2024. On a transect along 167°W, Conductivity, Temperature, and Depth (CTD) measurements are taken at degree intervals between -5°- 5° and in half degree intervals between -1°-1°. These measurements are supplemented with Underway CTD in quarter degree intervals between -2°-2° to have an increased resolution between these latitudes. Using the Thermodynamic Equation of Seawater, dynamic height is calculated using the dynamic height anomaly equation and used as a geostrophic streamfunction to predict velocities. Measurements from CTD casts are used to calculate the vertical profile of geostrophic velocity using the relative geostrophic velocity equation and compared to Acoustic Doppler Profiler (ADCP) measurements, which have been averaged at midpoint latitudes. These two vertical profiles are compared to determine the latitude-dependent variability in Root Mean Squared error values. Results indicate that as latitudes approach the equator, discrepancies between calculated geostrophic velocities and measured ADCP velocities increase, as evidenced by a latitude-dependent rise in root mean square (RMS) error values. External factors such as Equatorial Counter Current (ECC) and North Equatorial Counter Current (NECC) contribute to these discrepancies. This paper addresses the lack of Coriolis fore at the Equator by comparing calculations and measured velocity profiles to determine the error between them, identifying the accuracy of predictions made using latitude while nearing the Equator.

Plain Language Summary

In the ocean, the way water moves is influenced by a balance between Coriolis force and pressure gradient force, known as geostrophic balance. However, near the equator, where Coriolis forces are absent, using standard equations to predict ocean currents becomes challenging. This study, conducted during the TN427 research cruise on the R/V Thomas G. Thompson, aimed to understand how well we can predict currents near the equator. Measurements were taken along a straight path in the Pacific Ocean, involving Conductivity, Temperature, and Depth (CTD) measurements at various latitudes, supplemented with more detailed measurements in areas nearer to the equator. Using these measurements, dynamic height is calculated and used to calculate geostrophic velocity at midpoint latitudes between measurements. The calculated velocities were then compared with actual measurements obtained from Acoustic Doppler Profilers (ADCP) at the same midpoint latitudes. The findings revealed that as we get closer to the equator, the predictions of ocean currents using traditional methods become less accurate. Discrepancies between calculated and measured velocities increase, particularly due to external factors like Equatorial Counter Current (ECC) and North Equatorial Counter Current (NECC). This study iterates the limitations of current prediction models near the equator, emphasizing the need to consider additional factors beyond latitude. Understanding these obstacles is essential for improving the accuracy of ocean current predictions, especially in regions crucial for global climate dynamics and navigation.

Introduction

The Pacific Ocean is a region of importance in many areas such as climate and trade due to its size and complex currents. Oceans influence atmospheric circulation and manage heat storage and redistribution. Teleconnection patterns, which are large-scale climate anomalies that are correlated across significant distances, can lead to teleconnections that influence weather and climate conditions in remote regions. Knowledge of currents in the Equatorial Pacific Ocean can aid ship travel; mariners and navigators alike use information about the Equatorial Pacific currents to optimize routes, enhancing both the reliability and speed of sea transportation and trade. Understanding ocean current patterns and being able to predict them depends on several factors, with the main driving force being geostrophy.

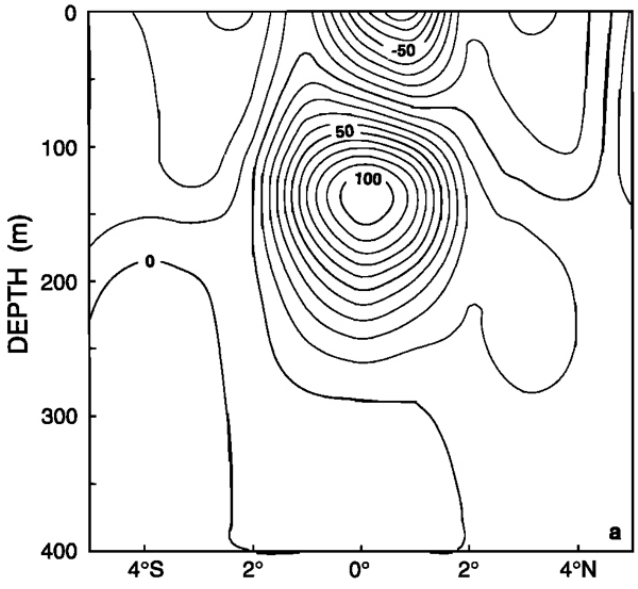

Figure 1. Geostrophic velocity taken across the equator between 4°S to 4°N, calculated at an averaged meridian from 150°W, 153°W, and 158°W. Contour interval is 10 cm s^{-1} with a positive eastward velocity. Figure from Cornuelle et al. 1993.

The most prominent subsurface currents in the Equatorial Pacific are the Equatorial Undercurrent (EUC) and the Equatorial Intermediate Current (EIC) (Johnson et al. 2002). The westward EIC flows under the EUC, which is present until around 250 m. These currents are located approximately between 1° north and south of the equator (Talley et al. 2011) around 100-200 m, a eastward flow represents the EIC. North of the EUC is the North Equatorial Current (NEC), located around 10-15°, and North Equatorial Counter Current (NECC), which extends from around 3-10°. The NECC relates to the EUC and has weaker current velocities than the NEC (Talley et al. 2011). The NECC can be seen in Figure 3 at 3-5°, with eastward velocities of around 10-20 cm/s. Another prevalent current in the area is the Equatorial Counter Current (ECC), which is a shallow surface current located around -2-2°. These currents flowing around the equator will affect surface current velocities in ways that are not predictable by geostrophy.

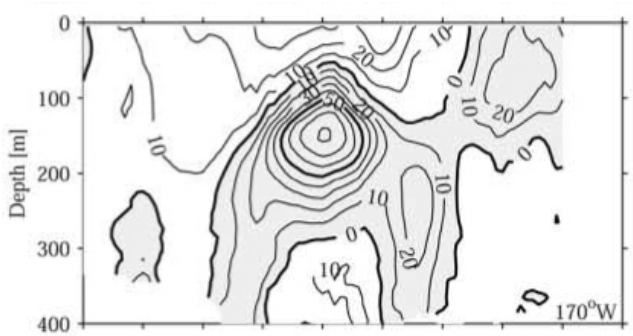

Figure 2. Mean zonal velocity at 170° W along the equator, from 8° S to 10°N. Contour interval is 10 cm s^{-1}, bolded contours at 50 cm s^{-1} intervals. Shaded velocities are eastward. Figure from Johnson et al. 2002.

The Equatorial Undercurrent and Equatorial Intermediate Current has been a subject of study regarding their adherence to geostrophic balance. Geostrophy establishes that a balance between

the Coriolis effect and the pressure gradient force produces predictable currents parallel to lines of constant pressure (Lukas and Firing 1984) and applying geostrophy here presents challenges. Talley et al. (2011) defined equations considering factors like temperature, salinity, and pressure from previous studies, however, all defined equations currently depend on Coriolis force. This is absent at the equator due to a latitude of 0°.

Coriolis force can be defined as an apparent force that acts on objects moving in a rotating system, such as the Earth. It results from the rotation of the Earth and affects the motion of fluids, including the atmosphere and oceans, and objects in motion relative to the rotating Earth. The Coriolis force arises due to the conservation of angular momentum. As the Earth rotates, different points on its surface move at different speeds depending on their distance from the axis of rotation. For example, points near the equator move faster than points near the poles. When an object moves in this rotating system, it experiences Coriolis force, which is perpendicular to both the velocity of the object and the axis of rotation (Persson, 1998). In the context of geostrophy, the deflection water experiences as a result of Coriolis force influences the direction of horizontal currents. The resulting geostrophic flow is perpendicular to both the pressure gradient force and the Coriolis force, leading to currents that flow parallel to lines of constant pressure.

Coriolis force, F_C, can be defined in Equation 1a, where m is mass, Ω is angular velocity, and v is tangential velocity. The Coriolis force is the actual force experienced by a moving object or fluid in a rotating reference frame. The Coriolis parameter (Equation 1b) is a simplified expression representing the Coriolis force per unit mass. It is used to describe the effect of the

Coriolis force in mathematical formulations of fluid dynamics and is a coefficient that reflects the strength of the Coriolis force at a specific location on Earth. It can be defined with Ω as the angular velocity of Earth and θ as the latitude at a given location.

$$F_C = -2m(\Omega \times v) \tag{1a}$$

$$f = 2\Omega \sin(\theta) \tag{1b}$$

When the Coriolis force and the pressure gradient force are in balance, it results in a state known as geostrophic equilibrium. In this equilibrium, the Coriolis force, which is influenced by the Earth's rotation, acts perpendicular to the pressure gradient force, which is directed from high to low pressure. These two forces balance each other, leading to a situation where there is no net acceleration of water. In the ocean, geostrophic equilibrium is observed in major ocean currents, where the water flows parallel to lines of constant sea level, also known as geostrophic contours (Persson, 1998). This balance between the Coriolis force and pressure gradient force is the cause of geostrophy.

$$-fv = -(1/\rho)\partial p/\partial x \tag{2a}$$

$$fu = -(1/\rho)\partial p/\partial y \tag{2b}$$

In the geostrophic balance equations defined by Eq. 2a and Eq. 2b by Talley et al. (2011), f is defined as the Coriolis parameter, v and u are directional velocity components in the north-south and east-west directions respectively, ρ is the density of the fluid, p is the pressure of the fluid, and x represents the eastward coordinate while y represents the westward coordinate.

Calculating geostrophy in the context of oceanography requires an equation of state to determine the pressure gradient force within the water column. In this study, the Thermodynamic Equation of Seawater 2010 (TEOS-10), is used in order to determine this force. TEOS-10 is a set of standardized equations and algorithms that provide a comprehensive representation of the thermodynamic properties of seawater, including its density and other essential parameters. The equations and algorithms were developed by the Intergovernmental Oceanographic Commission, International Association for the Physical Sciences of the Oceans, and the Scientific Committee on Oceanic Research to set a standard thermodynamic calculation for properties of seawater. TEOS-10 provides a complete thermodynamic representation of all properties of seawater as well as considers chemical composition and composition anomalies. Instead of using practical salinity, which is calculated from the conductivity of seawater, absolute salinity is used to accurately determine the horizontal density gradients. Horizontal density gradients are used to calculate dynamic height, which are then used to find geostrophic velocity (IOC, 2010).

$$fv = \frac{1}{\rho} k \times \nabla_z P = gk \times \nabla_p z \tag{3a}$$

$$k \times \nabla_{surf} \vartheta = f(v - v_{ref}) \tag{3b}$$

The geostrophic velocity equation is defined in TEOS-10 with Eq. 3a and 3b, where f is the Coriolis parameter, v is horizontal velocity, ρ is density, k is the vertical unit vector, g is gravity, and $\nabla_z P$ is the horizontal pressure gradient. In 3b, ϑ is defined as the geostrophic streamfunction, which in cases of isobaric pressure, is dynamic height. A streamfunction is a two-dimensional nondivergent flow with a constant value and describes the flow of a fluid. Dynamic height represents the height of a fluid column above a reference surface. The curl of the

streamfunction is proportional to the Coriolis effect and the velocity, and streamlines of the function represent the flow paths of the fluid. The difference between geostrophic velocity and geostrophic velocity at a reference pressure is defined as $(v - v_{ref})$, the horizontal velocity minus the horizontal velocity at a reference point (IOC, 2010). The importance of use of dynamic height as a geostrophic streamfunction in isobaric conditions where Root Mean Squared (RMS) error is improved by a factor of 16 in comparison to other streamfunctions.

Lukas and Firing (1984) determined the meridional momentum balance, consisting of geostrophic terms and other forces acting on the currents. With the sum of all forces acting on the currents, the effect geostrophic balance has on current direction can be determined, as well as the differences between predicted and measured velocities. With predicted current directions only considering geostrophy, using the meridional momentum balance equation to determine the magnitude of other forces acting on the currents can help investigate the expected differences between measured and determined velocity (Lukas and Firing, 1984).

I hypothesize geostrophic velocity predictions will show a latitude-dependent variability in RMS error values. As latitudes get closer to the equator, the RMS error values will increase with the lowest error at -5° and 5° and the highest RMS error values at 0°. The null hypothesis would be there is no difference between the RMS error values with latitudes farther from the equator in comparison to closer to the equator.

Methods

Measurements were taken on research cruise TN427 on the R/V Thomas G. Thompson, from 28 December 2023 to 11 January 2024. Conductivity, Temperature, and Depth (CTD) Rosette measurements from a Sea-Bird SBE 9 taken at every degree from 5°S to 5°N, and in half degrees from 1°S to 1°N across a meridional of 167°W. Salinities are reported on the TEOS-10 Absolute Salinity scale (IOC et al., 2010) with δS_A taken from version 3.0 of the McDougall et al. (2012) database. The CTD data was processed with the standard Sea-Bird SeaSoft data processing package following the GO-SHIP protocol (McTaggart et al. 2010) and reported in 2 db bins. The version of SeaSoft has implemented the TEOS-10 calculations.

Underway CTD (UCTD) measurements were taken from 2°S to 2°N in quarter degree intervals. Measurements were taken with a modified tow-yo method, where the UCTD sensor is deployed off the aft of the ship while traveling at 6 kts. The sensor is lowered for 3 minutes until it reaches around 300 m before being reeled to the surface. Unlike traditional tow-yos, a singular cast is deployed before moving to the next station. Casts were processed by M. Warner using a MatLab function provided by L. Rainville (personal communication).

Pressure, temperature, and absolute salinity are determined from measured CTD data. Using software routines provided by S. Hautala (personal communication) the data is extracted from the files and used to calculate dynamic height. With a python package that implements TEOS-10, the Dynamic Height Anomaly (DHA) is calculated with the following equation:

$$DHA = \int_{p_0}^{p} \frac{1}{\rho} dp \tag{4}$$

Where p is the pressure at a given depth, p_0 is the reference pressure, set to 600 m, ρ is the is the seawater density, which can be related to Absolute Salinity and Conservative Temperature through the Equation of State where S is the Absolute Salinity, T is Conservative Temperature, $\rho_0(S,T)$ is the reference density at the sea surface, and A, B, and K are coefficients.

$$\rho(S,T,p) = \rho_0(S,T)(1 - \frac{T-T_0}{K} + \frac{S-S_0}{A} + \frac{p-p_0}{B}) \tag{5}$$

The change in dynamic height between two stations, ΔDH, is divided by the distance between the two stations in km, Δy. This calculation represents the vertical shear at a depth z. The calculated shears represent midpoints between measured CTD stations, at latitudes every degree from 4.5°S to 4.5°N, and in quarter degrees from 0.75°S to 0.75°N.

ADCP data is collected during transect at 75 kHz using a shipboard ADCP, mounted on the hull of the R/V Thomas G. Thompson. The ADCP data was post-processed by Cody Cruz (personal communication) using UHDAS+CODAS software from the University of Hawaii (Firing et al. 2012). In addition to removing all periods beyond 5°S and 5°N to obtain a pure transect, threshold editing was applied to eliminate velocity values in bin ensembles with less than 80% good pings or greater than 500 mm/s error velocity magnitude. Phase correction was not warranted, but a final amplitude correction of 1.006 was applied, resulting in median water-track calibration bias estimates of 1.0005 for amplitude and 0.0525° for phase. Vertical ADCP profiles

are determined at midpoint latitudes through rounding of ADCP latitudes to 1 decimal place. In this instance, multiple vertical profiles may be rounded to the desired latitude. All profiles rounded to the desired midpoint are averaged to produce one profile for each latitude.

Using the equation of Relative Geostrophic Velocity (RGV), absolute geostrophic velocity can be calculated. For each latitude used to calculate the geostrophic shear, the shear at a depth of 600m is taken from ADCP velocity measurements. This is used as the reference velocity to integrate upwards through the water column to determine absolute geostrophic velocity, which can be determined by Equation 5.

$$u(_p) - u(_{p0}) = -\frac{g}{f} * (p0 - p)\frac{\Delta \mathrm{DH}}{\Delta \mathrm{y}} \tag{6}$$

Where $u(_p)$ is the absolute geostrophic velocity at a depth z, $u(_{p0})$ is the reference velocity, g is gravity, f is the Coriolis Parameter taken at the latitude each geostrophic shear profile is located at, $(p0 - p)$ is the difference between the reference depth and depth z, and $\frac{\Delta \mathrm{DH}}{\Delta \mathrm{y}}$ is the geostrophic shear at depth z. A modified version of this equation can be used to solve for geostrophic velocity in the u direction, where $\frac{\Delta \mathrm{DH}}{\Delta \mathrm{y}}_{p_{ref}}$ is the shear at a reference depth, and u_{ref} is the ADCP reference velocity at a reference depth.

$$u_{GEO} = \left(\frac{\Delta \mathrm{DH}}{\Delta \mathrm{y}} - \frac{\Delta \mathrm{DH}}{\Delta \mathrm{y}}_{p_{ref}}\right) * \frac{g}{f} + (u_{ref}) \tag{7}$$

Using the Equation 7, we can integrate upward through the water column at each location to determine the geostrophic velocity at each latitude. A reference depth of 600 m is chosen due to ADCP velocity plots ranging from 0 ~ 600 m (Figure 4). Once the ADCP reference velocity is

used to calculate absolute geostrophic velocity at 599 m, the absolute geostrophic velocity at 599 m is then used to calculate at 598 m, and so on. This continues until the entire column has been calculated, where the geostrophic velocity is the vertical antiderivative of the geostrophic shear. An alternate reference depth of 281 m is taken for calculating the absolute geostrophic velocity, as each cast reaches ~300 m and the lowest common depth of all casts is 281 m.

Error calculations were determined by calculating the RMS error of calculated geostrophic velocity compared to measured ADCP velocity. There are 40 pressure values in each ADCP profile, at varying depths, so the closest 40 values are taken from the geostrophic profile to calculate error. Using Equation 7, standard error is determined throughout the entire profile by subtracting geostrophic velocity from ADCP velocity. The absolute value is taken, and then the value is squared before the mean is calculated. The square root is taken of the value to determine RMS error.

$$RMS = \sqrt{\frac{\sum_{i=1}^{n}(|u_{ADCP} - u_{GEO}|^2)}{n}} \tag{8}$$

Results

The 20 plotted profiles can be divided into 4 groups: “Far”, “Approaching”, “Close”, and “Equator”. This is so analysis can be done on 4 geographic groupings rather than on 20 individual profiles. The 20 locations were grouped by their distance from the equator. Locations further than 3 degrees from the equator are labelled “Far”; locations between 1.5 and 2 degrees from the equator are labelled “Approaching”; locations between 0.8 and 1.5 degrees from the equator are labelled “Close”; and the “Equator” group includes locations within 0.8 degrees of

the equator. There are 4 vertical profiles in the Far and Approaching group, and 6 profiles in the Close and Equator groups. This is due to an increase in horizontal resolution when considering both CTD and UCTD data when approaching the equator.

Geostrophic velocities calculated using Equation 7 are plotted against depth to determine the vertical velocity profile. While the majority of the profiles are similar in velocity, ranging from around -0.5 m/s to 0.5 m/s, there are several anomalous profiles (Fig. 3). Midpoint latitudes -1.1°, -2.5°, 0.25°, 0.7°, 3.5° have a greater eastward velocity at depths 0-200m. Latitudes -1.4° and -0.25° have a higher positive magnitude of velocity at depths 100-400m. The rounded and averaged ADCP velocities shown in Figure 4 have a magnitude range of around -0.4 m/s to 0.3 m/s, and has an anomalous profile located at 2.5° ranging from 150-450m.

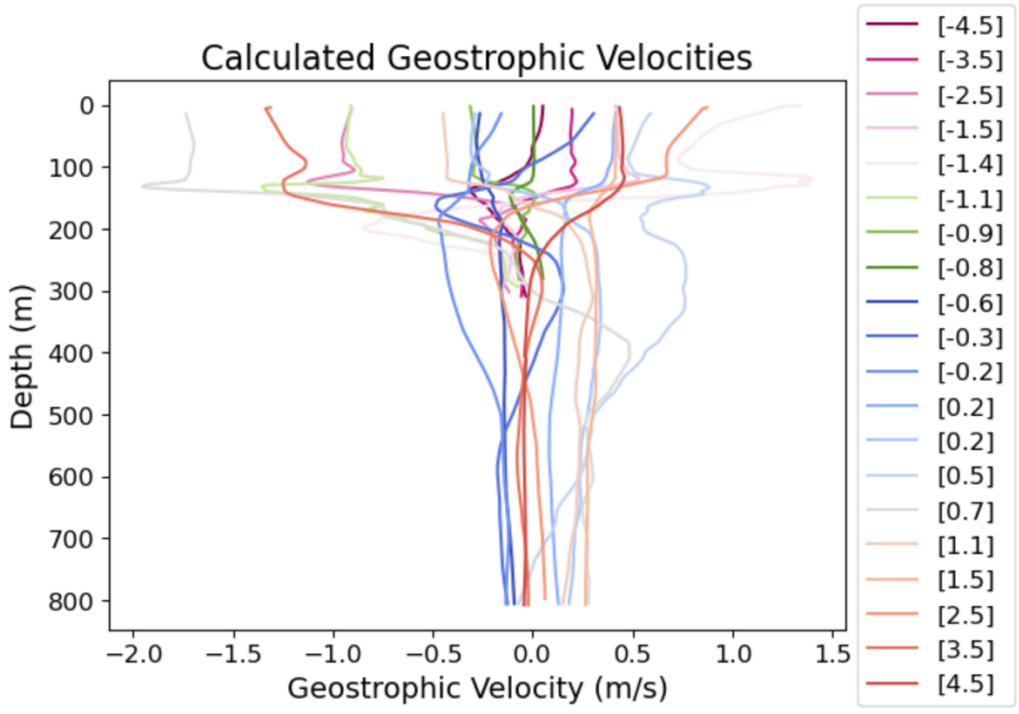

Figure 3. Geostrophic velocity of the water column at midpoint latitudes averaged between stations, calculated using Equation 7.

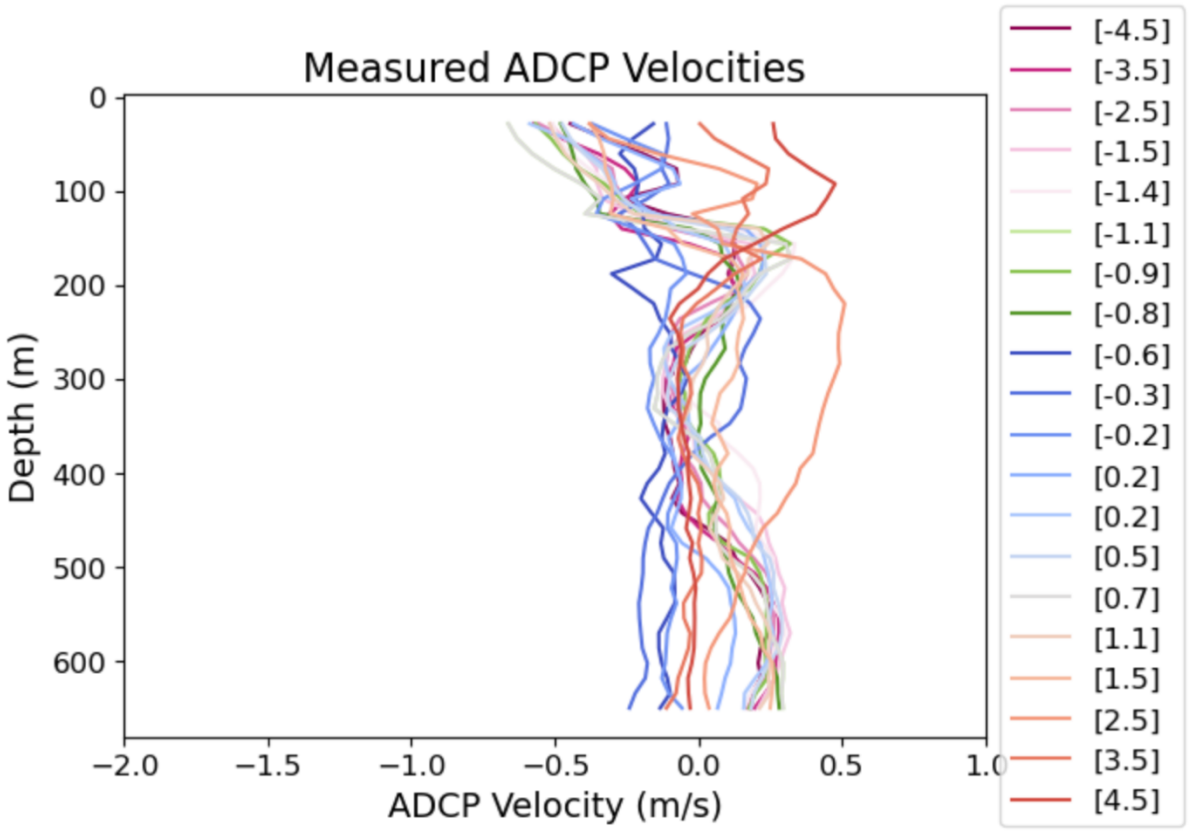

Figure 4. ADCP vertical velocity profiles, averaged through rounding, at midpoint latitudes averaged between stations.

The calculated geostrophic velocity profiles and measured ADCP profiles can be plotted against each other to identify discrepancies between the two profiles. Due to the combination of UCTD and CTD data for increased horizontal resolution, there is an overlap in midpoints where there are duplicate 0.2° values. These two profiles have been plotted against each other to determine an RMS error of 0.7251 (Fig. 5).

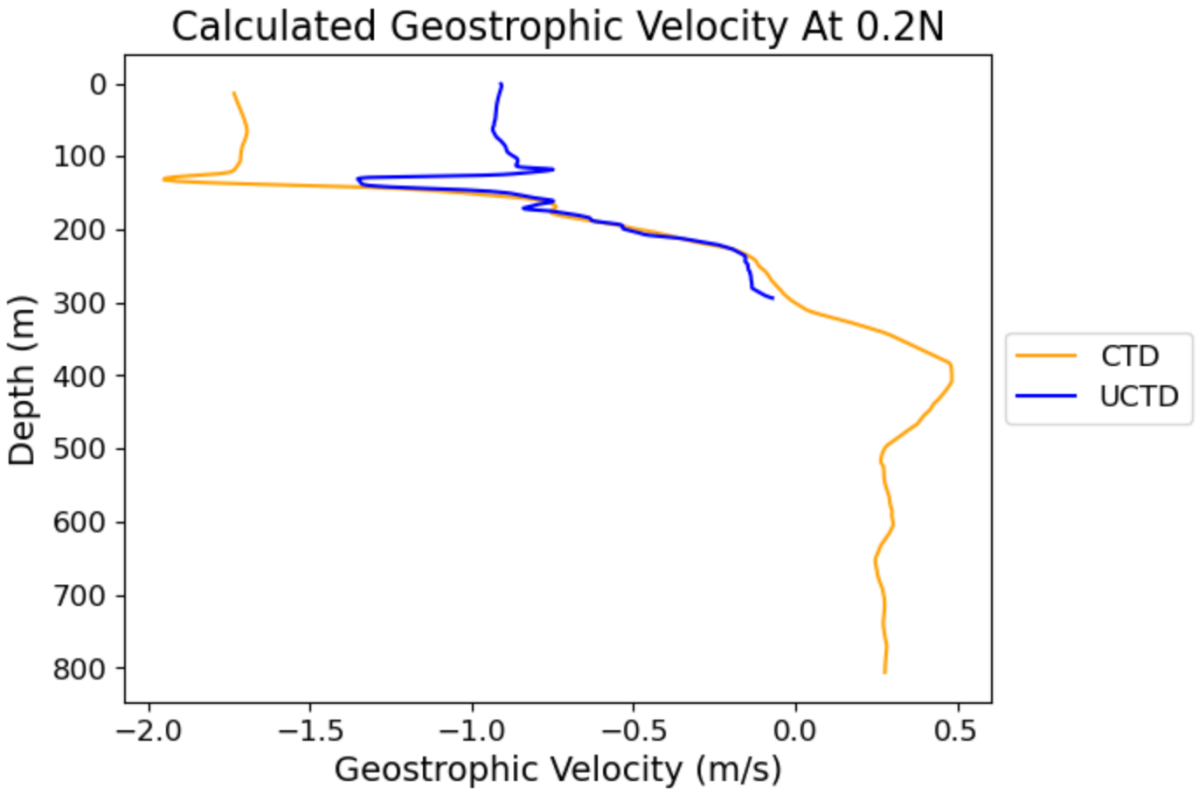

Figure 5. Geostrophic Velocity profiles at 0.2°, one profile calculated from CTD data and one profile calculated from UCTD data.

Figure 6 plots two midpoint latitudes from “Far”, “Approaching”, and “Equator”, one positive and one negative. These profiles represent their group, as they display the most common traits of their group. The Approaching group is chosen to represent both its own group and the Close group, as median latitudes between the Far and Equator groups share similar traits.

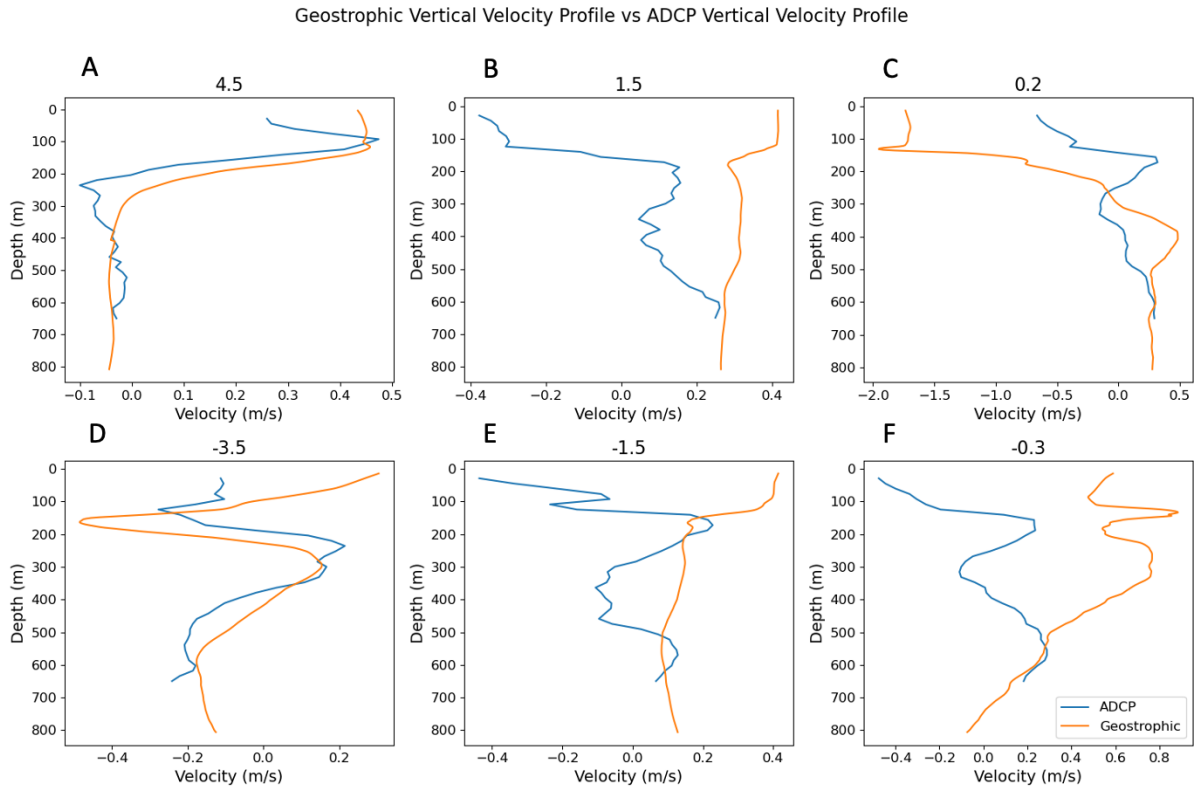

Figure 6. Geostrophic velocity plotted against ADCP velocity at Far, Approaching, and Equator latitudes. (A) 'Far' at midpoint latitude 4.5°. (B) 'Approaching' at midpoint latitude 1.5°. (C) 'Equator' at midpoint latitude 0.25°. (D) 'Far' at midpoint latitude -3.5°. (E) 'Approaching' at midpoint latitude -1.5°. (F) 'Equator' at midpoint latitude -0.25°.

RMS error is determined using Equation 8 and calculated for each latitude in Table 1. The RMS error for latitudes -4.5° and 4.5° are an order of magnitude smaller than the other latitudes and increases in value as the latitudes approach the equator. However, at latitudes 1.5°-3.5°, RMS error increases as latitudes move away from the equator.

Table 1. Midpoint latitudes and the RMS Error for all vertical geostrophic velocity profiles determined using Equation 8.

Latitude (°)	RMS Error (m/s)
-4.5	0.055
-3.5	0.163
-2.5	0.198
-1.5	0.286
-1.4	0.172
-1.1	0.295
-0.9	0.948
-0.8	0.223
-0.6	0.449
-0.3	0.588
-0.2	1.055
0.2_{UCTD}	0.956
0.2_{CTD}	0.672
0.5	0.398
0.7	0.181
1.1	0.212
1.5	0.361
2.5	0.511
3.5	0.669
4.5	0.085

Discussion

While geostrophic current directions cannot be calculated at the equator using the standard equation due to a latitude of 0 degrees, calculations are made at 0.2S and 0.2N, which is ~27.75 km on either side of the equator. While this is not directly on the equator, it is very close. Comparing calculated geostrophic velocities to measured ADCP velocity in Figure 5, for the "Far" group, it can be characterized as similar vertical velocity profiles with minor discrepancies, as the profiles follow a similar magnitude throughout the entire profile. For the "Approaching" and "Close" group, profiles can be characterized as having major discrepancies, and the "Equator" group can be characterized as having severe discrepancies. These generalizations of profiles help give a larger, overarching understanding about what happens to predictions when latitudes approach the equator—more discrepancies appear.

In order to verify this, we can analyze the RMS error. A lower RMS error suggests better agreement between predicted and measured data, and a higher RMS error suggests larger discrepancies. Table 1 lists the RMS error of each latitude, and a general trend can be identified that error increases as latitude approaches the equator. In Figure 9, there is an anomalous trend with latitudes 1.5°, 2.5°, and 3.5°, where RMS error increases moving away from the equator. There is also an abnormality located at -0.8°, where there is a sudden spike in RMS error value before the trend.

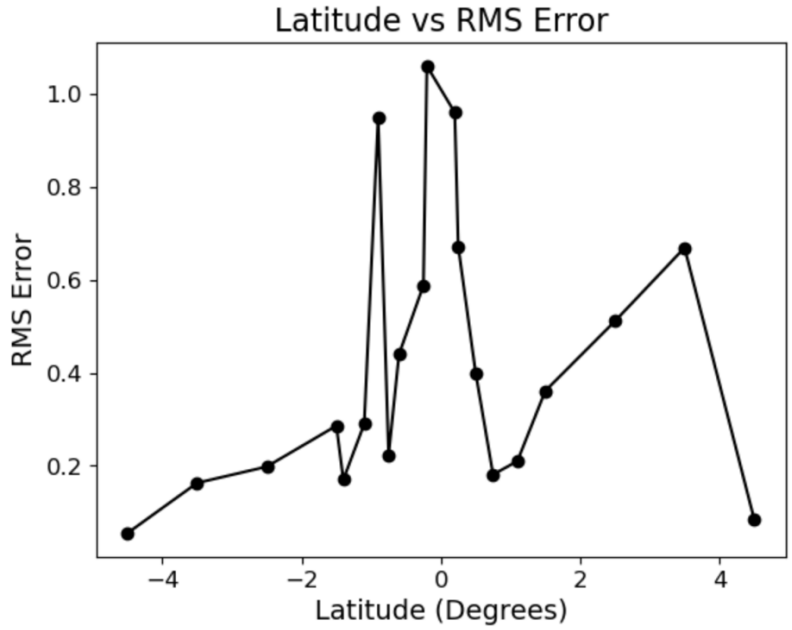

Figure 9. RMS errors (m/s) calculated using Equation 8 plotted against latitude.

There are several explanations for the discrepancy with these latitudes. The biggest factor on the differences between the measured velocities and the predicted velocities is the presence of the ECC and NECC. These currents are located around 2° to 3° and would have a major impact on the magnitude of the measured velocities (Talley et al. 2011). The presence of these currents, along with other external factors such as wind and eddies can cause discrepancies in data, as well as possible computational error, such as unit conversion errors or floating-point precision issues in Python calculations. Computational error or proximity to the equator could explain the anomaly at -0.8°.

Figure 5 shows the two vertical geostrophic profiles for midpoint latitudes at approximately the same location, one calculated using CTD data and one calculated using UCTD data. However, the RMS error for the difference between the two points is 0.7251. This could be due to a

computational error in which the entire CTD profile reaching ~800 m was compared to a UCTD profile of ~300 m. The two vertical velocity profiles appear to have the same shape, with differing magnitudes at different depths. Between depths of 150-300 m, the two profiles have nearly the same velocity magnitudes, but at depths of 0-150 m, the UCTD profile follows the same shape as the CTD profile, with larger magnitudes of velocity. This could be due to several reasons; Post processing of UCTD data could be inaccurate, causing the geostrophy calculations to be off due to variations in magnitude. The method of collecting UCTD data through a tow-yo rather than a stationary CTD cast could also influence the accuracy of the data. Without other overlapping latitudes, the cause of the discrepancy is not conclusive.

Based on measured information, it can be determined that the hypothesis is conclusive. The null hypothesis is disproven as there is a change in RMS error depending on latitude. Keeping in mind the anomalies present due to external forces such as the NECC and ECC, RMS error increases as latitudes approach the equator.

The comparison between geostrophic and ADCP velocities demonstrates the limitations of the geostrophic models outlined by Cornuelle et al. (1993). Analysis of RMS error reinforce the ideas that geostrophy will become increasingly difficult to predict as latitudes approach the equator. The error between calculated and determined velocities increase as latitudes approach the equator, due to a lack of Coriolis Force at the equator. Currently, all known equations for calculating geostrophy include latitude as geostrophy depends on latitude. Next steps to take would be to attempt predicting geostrophy without using latitude using known external factors.

The discrepancies determined align with Lukas and Firing's (1984) ideas that exterior forces such as wind stress, eddy viscosity, and currents play a crucial role in determining the direction and magnitude of equatorial currents. A major current located at 3.5° was enough to cause RMS error values to decrease moving away from the equator, opposite to the trend. Currents like these are not factored in geostrophy calculations, as they are outside factors not related to latitude. In the future, steps could be taken towards using gathered data and known locations of major currents and impacts on current velocity to improve the accuracy of velocity predictions using geostrophy.

Conclusions

This study on the effects of geostrophy on Equatorial Pacific currents has been driven by the effects these currents have on global climate dynamics, marine ecosystems, and navigation, among other effects. Geostrophy serves as a foundation for understanding oceanic circulation. Prior to this study, existing knowledge recognized the difficulty of applying geostrophic balance near the equator due to the absence of Coriolis force. Calculated findings show that RMS error of calculated geostrophic velocity and measured ADCP velocity does increase as latitudes approach the equator, with lowest errors at points furthest from the equator.

To further advance our understanding of Equatorial Pacific currents, it is important to acknowledge and address the limitations in this study. Future research should refine geostrophic models, considering the influence of external ageostrophic forces like wind, eddy viscosity, and currents. Further investigation into potential sources of error, such as unit conversions and

floating-point precision, will contribute to more accurate predictions. With consideration of known external ageostrophic forces, predictions of velocity will become more accurate.

Given the role of the Equatorial Pacific in global climate dynamics, ongoing research has important implications for climate predictions, ecological processes, and navigation strategies in this region. A comprehensive understanding of Equatorial Pacific currents is not only important for addressing existing challenges but also lays the foundation for more informed decisions and predictions in the face of a changing climate and evolving marine environments.

Acknowledgements

I express my sincere gratitude to Captain and the crew of the R/V Thomas G. Thompson, with special appreciation for the Marine Technicians, for their invaluable assistance in handling the UCTD. I extend my thanks to Professor Mark Warner for his guidance and support throughout the proposal and thesis process, including the processing of UCTD data. Special appreciation goes to Professor Susan Hautala for her assistance in CTD processing and her insightful advice on my proposal, as well as Professor Georgy Manucharyan for his assistance in correcting my code and for providing guidance on my thesis. My appreciation extends to Cody Cruz for his assistance with code, data processing, and valuable advice whenever needed. I am grateful to Mina Cheney for her continuous discussions on thesis writing and Emma Nguyen for her patience and support during my seasickness on the cruise. Lastly, I would like to express my gratitude to Yanfeng Shao for late-night WeChat discussions, collaborating on thesis writing sections, and providing valuable insights.

References

Bryden, H.L. and Brady, E.C. (1985) Diagnostic model of the three-dimensional circulation in the upper equatorial Pacific Ocean, *Journal of Physical Oceanography*, 15(10), pp. 1255–1273. doi:10.1175/1520-0485(1985)015<1255:dmottd>2.0.co;2.

Cornuelle, B. D., Morris, M. Y., & Roemmich, D. H. (1993). An objective mapping method for estimating geostrophic velocity from hydrographic sections including the Equator. *Journal of Geophysical Research: Oceans*, *98*(C10), 18109–18118. https://doi.org/10.1029/93jc01729

Firing, E., J. Hummon, and T. Chereskin (2012), Improving the quality and accessibility of current profile measurements in the Southern Ocean, Oceanography, 25(3), 164–165, doi:10.5670/oceanog.2012.91.

IOC, SCOR & IAPSO (2010). The international thermodynamic equation of seawater - 2010: Calculations and use of thermodynamic properties. *Intergovernmental Oceanographic Commission, Manuals and Guides No. 56*, UNESCO (English), 196 pp

Johnson, E. S., & Luther, D. S. (1994). Mean zonal momentum balance in the upper and central equatorial Pacific Ocean. *Journal of Geophysical Research: Oceans*, *99*(C4), 7689–7705. https://doi.org/10.1029/94jc00033

Johnson, G. C., Sloyan, B. M., Kessler, W. S., & McTaggart, K. E. (2002). Direct measurements of upper ocean currents and water properties across the tropical Pacific during the 1990s. *Progress in Oceanography*, *52*(1), 31–61. https://doi.org/10.1016/s0079-6611(02)00021-6

Joyce, T. M., Lukas, R., & Firing, E. (1988). On the hydrostatic balance and equatorial geostrophy. *Deep Sea Research Part A. Oceanographic Research Papers*, *35*(8), 1255–1257. https://doi.org/10.1016/0198-0149(88)90081-7

Lukas, R., & Firing, E. (1984). The geostrophic balance of the Pacific Equatorial Undercurrent. *Deep Sea Research Part A. Oceanographic Research Papers*, *31*(1), 61–66. https://doi.org/10.1016/0198-0149(84)90072-4

McDougall, T.J., Jackett D. R., Millero F. J., Pawlowicz R. & Barker P. (2012). A global algorithm for estimating Absolute Salinity, *Ocean Sci., 8*, 1123–1134

Moum, J. N., R.-C. Lien, A. Perlin, J. D. Nash, M. C. Gregg, and P. J. Wiles. 2009. Sea surface cooling at the equator by subsurface mixing in tropical instability waves. *Nature Geoscience 2*: 761–765. doi:10.1038/ngeo657

Persson, A. (1998). How do we understand the coriolis force? *Bulletin of the American Meteorological Society*, *79*(7), 1373–1385. https://doi.org/10.1175/1520-0477(1998)079<1373:hdwutc>2.0.co;2

Picaut, J., & Tournier, R. (1991). Monitoring the 1979-1985 equatorial Pacific current transports with expendable Bathythermograph Data. *Journal of Geophysical Research: Oceans*, *96*(S01), 3263–3277. https://doi.org/10.1029/90jc02066

Talley, L. D., Pickard, G. L., Emery, W. J., & Swift, J. H. (2011). *Descriptive physical oceanography: An introduction*. Academic Press.